Spectral Analysis of Orbits via Discrete Fourier Transforms

C. Hunter (hunter@math.fsu.edu)
Department of Mathematics, Florida State University, Tallahassee, Florida 32306-4510, USA

Abstract.
We give some simple and direct algorithms for deriving the Fourier series which describe the quasi-periodic motion of regular orbits from numerical integrations of those orbits. The algorithms rely entirely on discrete Fourier transforms. We calibrate the algorithms by applying them to some orbits which were studied earlier using the NAFF method. The new algorithms reproduce the test orbits accurately, satisfy constraints which are consequences of Hamiltonian theory, and are faster. We discuss the rate at which the Fourier series converge, and practical limits on the degree of accuracy that can reasonably be achieved.

Keywords: Hamiltonian Dynamics, Orbits, Fourier Analysis

1. Introduction

This work develops efficient and accurate methods for computing Fourier expansions of orbits in potentials of galactic type. Their ultimate purpose is for use in constructing stellar dynamic models. Efficient methods are needed because galactic models require the use of large numbers of orbits. The methods described here are designed specifically for regular orbits, and may be useful also with nearly regular orbits whose characteristics change slowly with time. This is not to suggest that regular and near-regular orbits are the only ones of interest in galactic dynamics – they are not. But regular orbits can be an important component of galaxies, and this work is relevant to them at least.

The methods to be described use Fourier analysis. Fourier analysis of orbits in galactic-type potentials was pioneered by Binney and Spergel (1982, 1984). There has been a recent upsurge of interest as a result of the work of J. Laskar (1990, 1993, 1999) who has developed accurate numerical methods of Fourier analysis which are known by the acronym NAFF (Numerical Analysis of Fundamental Frequencies). These methods were developed originally for solar system phenomena, including mildly chaotic ones, but they were also applied by Papaphilippou and Laskar (1996, 1998) to potentials of galactic type. Other applications of NAFF to cuspy triaxial galactic-type potentials have followed, including those by Carpintero and Aguilar (1998), Valluri

and Merritt (1998), Wachlin and Ferraz-Mello (1998), and Merritt and Valluri (1999). Copin, Zhao and de Zeeuw (2000) have that smooth orbital densities can be derived from Fourier representations of orbits obtained using NAFF, and have illustrated the method on a Stäckel potential.

NAFF begins with the numerical integration of an orbit, and the recording of its phase space coordinates at a sequence of equally spaced time steps. A discrete Fourier transform (DFT) is applied to this data, and the most prominent frequency is identified as that belonging to the largest Fourier coefficient [c.f. Binney and Spergel (1982)]. This provides an initial estimate of the most prominent frequency. This estimate is refined by the use of Fourier integrals and window functions. The refined frequency is that which maximizes the Fourier integral which represents the amplitude associated with that frequency. This component is then subtracted out, and subsequent Fourier components are identified sequentially in order of diminishing prominence, and subtracted in turn.

This work provides an alternative way of performing the Fourier analysis entirely with discrete transforms. It is natural to seek such a method because the continuous orbit is discretized by the initial numerical integration, and it is hard to see what can be gained by switching to Fourier integrals subsequently. We describe our method in Section 3, after first reviewing some essential elements of Hamiltonian Dynamics in Section 2. We calibrate it in Section 4 by applying it to three cases discussed in detail by Papaphilippou and Laskar (1996). In Section 5 we compare our method with that of Laskar, and give our conclusions. An appendix justifies a key aspect of our method of determining frequencies of Fourier components in a time series.

2. Hamiltonian Dynamics

A regular orbit in a system with n degrees of freedom lies on an n-torus in phase space (Binney and Tremaine 1987). It is generally quasi-periodic, and has n fundamental frequencies which we label as ν_1 to ν_n. The position vector of the orbit has the Fourier representation

$$\mathbf{x}(t) = \sum_{\mathbf{k}} \mathbf{X}_{\mathbf{k}}(\mathbf{I}) e^{i(\mathbf{k}\cdot\nu)t}. \tag{1}$$

where ν is the n-vector of the fundamental frequencies, and $\mathbf{k}$ is an n-vector with integer components. Summation is over all such integer vectors $\mathbf{k}$. The Fourier coefficients $\mathbf{X}_{\mathbf{k}}$ are functions of the actions $\mathbf{I}$. Actions and their conjugate angles ϕ form a canonical set of variables,

in terms of which the Hamiltonian is $H(\mathbf{I})$ and independent of the angles. The value of the action vector is constant for each specific orbit, Consequently the angle ϕ_j increases uniformly with time at the rate $\nu_j = \partial H/\partial I_j$. The phase space variables of position and velocity have Fourier representations in the action-angle variables $(\mathbf{I}, \phi)$ which are given by the equations

$$\mathbf{x} = \sum_{\mathbf{k}} \mathbf{X_k}(\mathbf{I}) e^{i\mathbf{k}\cdot\phi}, \quad \mathbf{v} = \sum_{\mathbf{k}} i(\mathbf{k}\cdot\nu)\mathbf{X_k}(\mathbf{I}) e^{i\mathbf{k}\cdot\phi}. \tag{2}$$

Here we either require that each angle ϕ_j be zero at time $t = 0$, or else absorb extra constant terms into the definitions of the Fourier coefficients $\mathbf{X_k}(\mathbf{I})$.

Fourier series are strongly constrained by orbital symmetries, and the Hamiltonian. Specifically

$$I_j = \frac{1}{2\pi} \oint_{\mathcal{C}_j} \mathbf{v} \cdot d\mathbf{x}, \tag{3}$$

where $\mathcal{C}_j$ is a circuit around the torus of constant $\mathbf{I}$, and which is such that the angle ϕ_j increases by 2π, but other angles are unchanged. Then

$$I_j = \sum_{\mathbf{k}} k_j(\mathbf{k}\cdot\nu)\mathbf{X_k}\cdot\mathbf{X_{-k}} = \sum_{\mathbf{k}} k_j(\mathbf{k}\cdot\nu)|\mathbf{X_k}|^2, \tag{4}$$

while

$$\sum_{\mathbf{k}} k_j(\mathbf{k}\cdot\nu)\mathbf{X_k}\cdot\mathbf{X_{m-k}} = 0, \tag{5}$$

where $\mathbf{m}$ is a non-zero integer vector with zero j'th component (Binney and Spergel 1984).

3. Implementing NAFF the Discrete Transform Way

3.1. Discrete Transforms and Windows

We use a centered time interval and integrate from time $t = -T$ to $t = T$, with positions and velocities recorded at $2N$ equally spaced times in steps of $\Delta t = T/N$. The discrete Fourier coefficients of a function $f(t)$ are calculated from its tabulated values as

$$F_k = \frac{1}{2N} \sum_{n=1-N}^{N} f(n\Delta t) e^{-\pi i n k/N}, \tag{6}$$

for $k = 1-N$ to N, and can be computed using a fast Fourier transform. We use the average $\frac{1}{2}[f(T) + f(-T)]$ when evaluating $f(T)$ in this

formula (Briggs and Henson 1995). Then consistently $f(t)$ is periodic of period $2T$ in t and F_k is periodic of period $2N$ in k. We use the same window functions

$$\chi_p\left(\frac{t}{T}\right) = \frac{2^p(p!)^2}{(2p)!}\left(1+\cos\frac{\pi t}{T}\right)^p, \tag{7}$$

as Laskar. These window functions taper to zero at the ends of the interval $[-T,T]$ with increasing rapidity for increasing values of p. They are ideally suited to the DFT. This is because

$$1+\cos\frac{\pi t}{T} = \frac{1}{2}e^{i\pi t/N\Delta t} + 1 + \frac{1}{2}e^{-i\pi t/N\Delta t}. \tag{8}$$

Hence the DFT of $f(t)\chi_1(t/T)$ is simply derived from that of $f(T)$ as

$$F_k^{(1)} = \frac{1}{2}F_{k-1} + F_k + \frac{1}{2}F_{k+1}. \tag{9}$$

The Fourier coefficients of f multipled by window functions of any order, $f(t)\chi_p(t/T)$, can be computed iteratively with minimal effort using the recursive relation

$$F_k^{(p)} = \frac{p}{2p-1}\left[\frac{1}{2}F_{k-1}^{(p-1)} + F_k^{(p-1)} + \frac{1}{2}F_{k+1}^{(p-1)}\right], \qquad F_k^{(0)} = F_k. \tag{10}$$

3.2. Estimating Frequencies

The essential purpose of the Fourier analysis is to identify the elementary frequency components of $f(t)$. We now consider such a component $g(t) = e^{i\nu t}$, and its windowed Fourier coefficients. We denote the latter as $G_k(\nu)$. They are calculated from $g(t)$ in the same way as in equation (6), and we obtain

$$G_k(\nu) = \frac{\sin\theta}{2N\tan(\frac{\theta}{2N})} = S(\theta), \quad \text{where} \quad \theta = \nu T - k\pi. \tag{11}$$

This equation defines the function $S(\theta)$ which is the discrete analog of the sinc function which arises with continuous Fourier transforms, and to which it indeed tends as $N \to \infty$. It is even and periodic of period $2N\pi$ in θ, and vanishes at all integer multiples of π, except for those which are also integer multiples of $2N\pi$. The windowed Fourier coefficients of $g(t)$ can also be calculated iteratively and are

$$\begin{aligned} G_k^{(p)}(\nu) = S^{(p)}(\theta) &= \frac{p}{2p-1}\left[\frac{1}{2}S^{(p-1)}(\theta+\pi) + S^{(p-1)}(\theta)\right. \\ &\quad \left. + \frac{1}{2}S^{(p-1)}(\theta-\pi)\right], \\ S^{(0)}(\theta) &= S(\theta). \end{aligned} \tag{12}$$

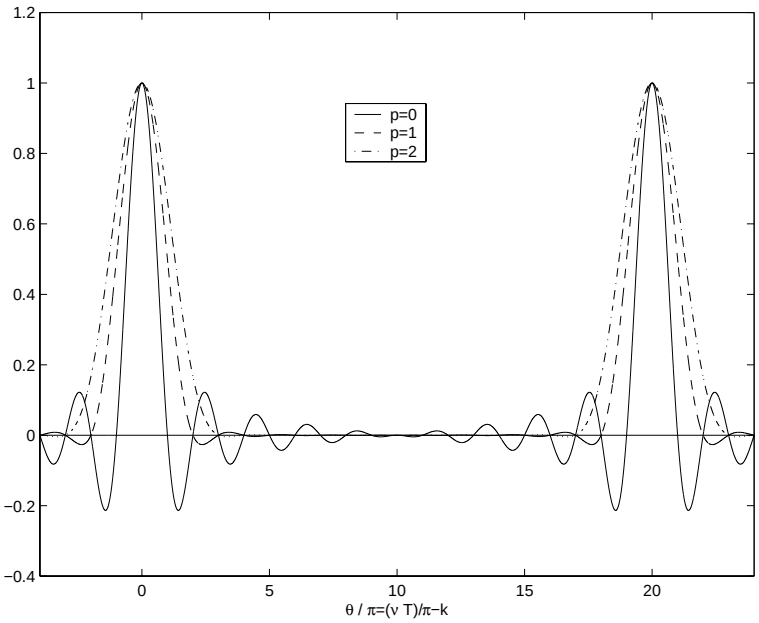

Figure 1. Fourier transforms $G_k^{(p)}(\nu) = S^{(p)}(\theta)$ of a simple exponential $e^{i\nu t}$ with no windowing ($p = 0$) and with the first two window functions (7) for $N = 10$

An explicit expression for the DFT of $g(t)\chi_1(t/T)$ is

$$G_k^{(1)}(\nu) = \frac{\sin\theta}{2N\tan(\frac{\theta}{2N})\left[1-\sin^2(\frac{\theta}{2N})/\sin^2(\frac{\pi}{2N})\right]}, \tag{13}$$

The DFT of $g(t)$ and of $g(t)$ multiplied by the first two of the window functions (7) are shown in Fig. 1. With increasing p the central peaks become successively wider while the side lobes decay increasingly rapidly so that frequencies increasingly stand out from the background. Fig. 1 is plotted for the impractically small value of $N = 10$ to emphasize the periodicity of period $2N$ of all discrete Fourier coefficients. As N becomes large, the discrete Fourier coefficients approach the limits

$$\lim_{N\to\infty} G_k^{(p)}(\nu) = \frac{\sin\theta}{\theta\prod_{j=1}^{p}\left(1-\frac{\theta^2}{j^2\pi^2}\right)}. \tag{14}$$

Although the DFT in Fig. 1 are plotted for continuous ranges of their arguments, they are of course known only at discrete values of θ which are π apart in any application.

We estimate unknown frequencies ν using ratios of adjacent Fourier coefficients. This idea is due to Lanczos (1956) who used it with the

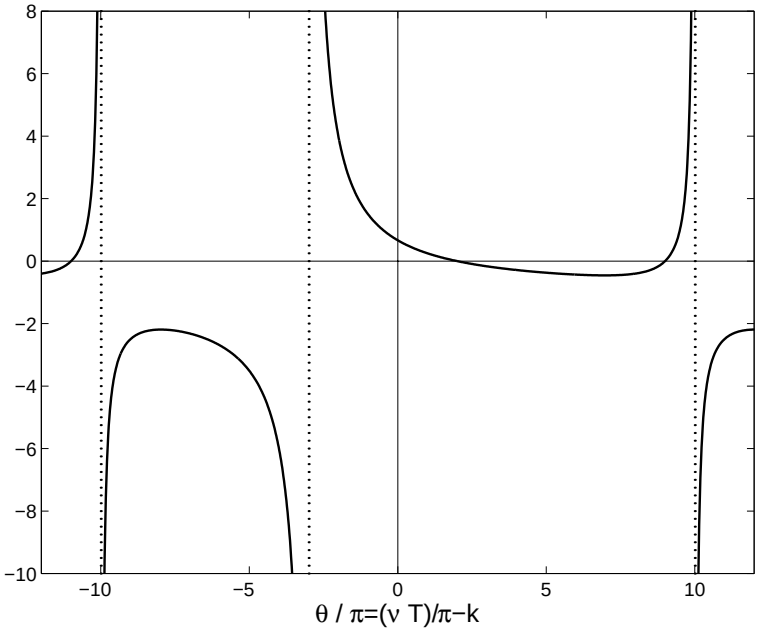

Figure 2. Ratio of two adjacent finite transforms $G^{(2)}_{k-1}(\nu)/G^{(2)}_k(\nu)$ as functions of $\theta = \nu T - k\pi$ for $N = 10$. The ratio is approximately $(p\pi - \theta)/[\theta + (p+1)\pi]$ for large N.

$p = 1$ (Hanning) window function. It was rediscovered by Carpintero and Aguilar (1998) who used it without windowing ($p = 0$). We use it without restriction on p as follows. We look for a prominent frequency by locating a range of k values where the Fourier coefficients F_k are relatively large, and humps similar to those shown in Fig. 1 develop. As Fig. 2 implies, the ratios $F^{(p)}_{k-1}/F^{(p)}_k$ are positive for a limited range of k values. We select some k for which the ratio is positive and equal to C say. We then find the frequency ν for which the ratio $G^{(p)}_{k-1}(\nu)/G^{(p)}_k(\nu)$ has the same ratio C. This gives us an equation

$$\frac{G^{(p)}_{k-1}(\nu)}{G^{(p)}_k(\nu)} = \frac{S^{(p)}(\theta+\pi)}{S^{(p)}(\theta)} = C, \tag{15}$$

for θ. We show in the Appendix that it is in fact a polynomial equation of degree $2p$ in $\tau = \tan(\theta/2N)$. One need not compute all its roots, all but two of which are complex for positive C (c.f. Fig. 2), because $S^{(p)}(\theta+\pi)/S^{(p)}(\theta)$ becomes negative outside the range $-(p+1)\pi \le \theta \le p\pi$ where the numerator and denominator are out of phase. Hence we need only the small real root for τ which lies in the narrow range $-(p+1)\pi/2N \le \theta/2N \le p\pi/2N$. From τ, we have θ and then the

Table I. Two sets of estimates of the frequency of from $T = 20$ integrations of the x-axis orbit with $E = -.4059$ in the logarithmic potential (17) of Section 4.1. The value 2.1390519547 is accurate.

	$N = 256$		$N = 512$
p	ν	p	ν
1	2.1390476260	1	2.1390476324
2	2.1390519936	2	2.1390519918
3	2.1390519526	3	2.1390519541
4	2.1390519586	4	2.1390519547
5	2.1390520877	5	2.1390519547
6	2.1390523943	6	2.1390519547
7	2.1390528801	7	2.1390519547
8	2.1390535210	8	2.1390519547

frequency $\nu = (\theta + k\pi)/T$. These estimates should become increasingly accurate with increasing p, as the sidelobes decay and individual frequencies stand out. One can easily test whether this is the case by checking for consistency between estimates at neighboring values of k, and by calculating a sequence of estimates for successive increments of p, and checking whether they converge. Table 1 shows the results of two analyses of the x-axis orbit discussed in Section 4.1, using the same integration interval but different spacings. The right hand set show consistent convergence to the true frequency, while the left hand set lack consistency, although getting quite close at $p = 4$,

3.3. Aliasing

Aliasing is an unavoidable consequence of discretization. Two components $e^{i\beta t}$ and $e^{i\gamma t}$ are indistinguishable on the grid specified in Section 3.1 if $(\beta - \gamma)\Delta t = 2m\pi$ for any integer m. From a practical point of view, two components may interfere and complicate our method for determining frequencies when $(\beta - \gamma)\Delta t/2\pi$ is *close* to an integer. That is the reason for the lack of convergence in the left hand column of Table 1. The aliasing there is between the fundamental frequency ν and its harmonics with frequencies 37ν and 39ν because $38\nu\Delta t/2\pi = 1.0107$. (Because x is real, all frequencies occur in $\pm$ pairs.) The G_k for the fundamental frequency peaks between $k = 13$ and $k = 14$, while those for the two harmonics peak near $k = 8$ and $k = 19$ respectively. Both of these peaks are much lower because their amplitudes are $A_{19} = .301 \times 10^{-4}$ and $A_{20} = .235 \times 10^{-4}$, whereas

$A_1 = .8622$. Nevertheless the lower peaks spread with increasing p (see Fig. 1) and cause the improvement of the estimates of ν to stop after $p = 4$. Aliasing can always be overcome by increasing N and decreasing Δt and moving the peaks further apart. As the second column of Table 1 shows, doubling the number of data points in an interval of the same length removes the difficulty.

3.4. Determining Amplitudes

By working with ratios, the amplitude of a Fourier component has no influence on the estimation of the frequency. However, once one has an accurate estimate of that frequency, one can estimate its amplitude in $f(t)$, and that of its conjugate $e^{-i\nu t}$, by

$$A_\nu = \frac{F_k^{(p)}}{G_k^{(p)}(\nu)}, \quad A_{-\nu} = \frac{F_\ell^{(p)}}{G_\ell^{(p)}(-\nu)}, \tag{16}$$

respectively.

The iterated Fourier transforms of $f(t) - A_\nu e^{i\nu t} - A_{-\nu} e^{-i\nu t}$, that is of $f(t)$ with the dominant frequency removed, are $F_k^{(p)} - A_\nu G_k^{(p)}(\nu) - A_{-\nu} G_k^{(p)}(-\nu)$. Note that $G_k^{(p)}(-\nu) = G_{-k}^{(p)}(\nu)$. The only additional work needed here is that of calculating the values of $G_k^{(p)}(\nu)$ with the chosen ν for all k in $[-N, N]$. Then one can repeat the procedure iteratively to estimate as many frequencies and amplitudes as needed.

One can modify this step-by-step procedure once the n fundamental frequencies have been determined by assuming that all subsequent frequencies are combinations $\mathbf{k} \cdot \nu$ suitable to that orbit (see Section 4). These amplitudes can be calculated systematically by applying equation (16) near a peak of $G_k^{(p)}$ and then subtracting. One should subtract in at least approximate order of magnitude. Once one has a set of frequencies and amplitudes, their accuracy can be checked by evaluating the truncated Fourier series and comparing with the tabulated values of f from which it was derived.

4. Applications

We test the DFT method on orbits in the logarithmic potential

$$\Phi(x, y) = \ln\left(R_c^2 + x^2 + \frac{y^2}{q^2}\right), \tag{17}$$

with flattening $q < 1$ and a core radius R_c (Binney and Tremaine 1987). We investigate the same three orbits for the case $R_c = 0.1$ and $q = 0.9$

to which Papaphilippou and Laskar (1996), hereafter PL, applied their NAFF procedures.

4.1. One-dimensional orbits

Though simple dynamically, x-axis orbits for which $y \equiv 0$ provide an excellent opportunity for testing the methods of Section 3 because true values can be computed with high precision. The position vector of an orbit which starts at $x = 0$ at time $t = 0$ has the Fourier representation

$$x(t) = \sum_{j=1}^{\infty} A_j \sin(2j-1)\nu t. \tag{18}$$

The frequency ν for an orbit of energy E is

$$\frac{\pi}{\nu} = \sqrt{2}\int_0^{x_{\max}} \frac{dx}{\sqrt{E - \Phi(x,0)}}, \qquad \Phi(x_{\max},0) = E. \tag{19}$$

The Fourier series is a sine series because of the initial conditions, and with odd multiples of νt only because of the evenness of Φ in x. Estimates of the coefficients A_j, which are all positive, can be compared with exact values computed from

$$A_j = \frac{4\nu}{\pi}\int_0^{\pi/2\nu} x(t)\sin(2j-1)\nu t\, dt. \tag{20}$$

PL give frequencies and amplitudes for the orbit which starts at $x = 0.49$ with $v = 1.4$, and hence $E = -.4059$. The right column of Table 1 gives our determination its frequency, while Fig. 3b plots the Fourier coefficients. After an initial steep decline ($A_2/A_1 = .076$), the rate of decay of A_j with increasing j decreases, and $A_{25}/A_{24} = .798$ at the edge of the plot. This is because x needs many sine terms to describe its time variation accurately, and, correspondingly, the phase-plane trajectory of Fig. 3a is not elliptical. The slow decay of the A_j coefficients does not, as PL suggest, indicate any inaccuracy in the representation in action/angle variables. In fact it is related to the small magnitude of the core radius R_c as we now show. The Fourier series (18) of the analytic function $x(t)$ become the Laurent series

$$x = \sum_{j=1}^{\infty} \frac{i}{2} A_j \left[-\zeta^{2j-1} + \frac{1}{\zeta^{2j-1}}\right] \tag{21}$$

in the variable $\zeta = e^{i\nu t}$ (Davis, 1975). This series converges in an annular region of the complex ζ-plane, which includes the physical orbit on which $|\zeta| = 1$. However, it is singular at the two real values of ζ for

which $x = \pm iR_c$ and the logarithmic potential is infinite. We locate these points by integrating the energy equation, written for $x = iw$, from $t = 0$ where $w = 0$ and $\zeta = 1$, to $w = R_c$. We find that the singularity lies at $\zeta = \zeta_c$ where

$$\zeta_c = \exp\left[\frac{\nu}{\sqrt{2}} \int_0^{R_c} \frac{dw}{\sqrt{E - \ln(R_c^2 - w^2)}}\right]. \tag{22}$$

Integrating in the direction of decreasing ζ shows that there is a matching singularity where $w = -R_c$ at $\zeta = 1/\zeta_c$. Hence the Laurent series (21) converges only in the annulus $1/\zeta_c < |\zeta| < \zeta_c$, which implies (Davis, 1975) that

$$\lim_{j\to\infty} \frac{A_{j+1}}{A_j} = \frac{1}{\zeta_c^2}. \tag{23}$$

The numerical value of this limit for the PL orbit is 0.8702, and this is the limit to which the ratios of the A_j plotted in Fig. 3b are gradually climbing.

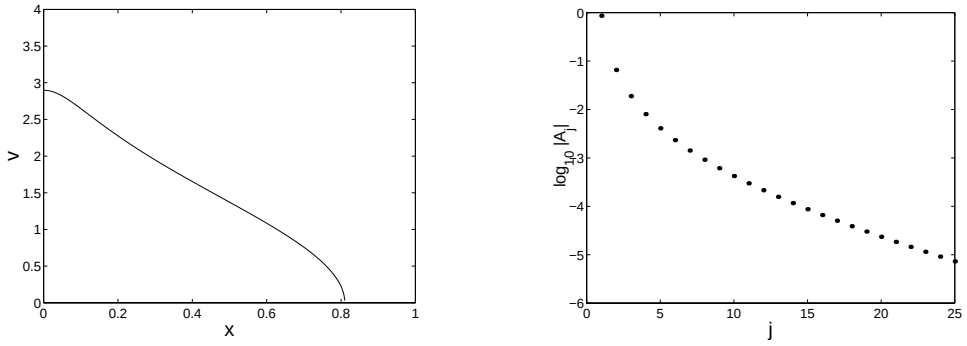

a. The phase plane b. Fourier coefficients

Figure 3. The x-axis orbit at energy E=-.4059

4.2. Two-dimensional orbits

The evenness of the potential (17) restricts the two-dimensional Fourier series too. When ν_1 is the fundamental frequency of the oscillation in x, and ν_2 is the frequency of that in y, then the Fourier expansions are

$$\begin{aligned} x &= \sum_{j=-\infty}^{\infty} \sum_{k=-\infty}^{\infty} A_{j,k} e^{i[(2j+1)\nu_1 + 2k\nu_2]t}, \quad A_{-j-1,-k} = \bar{A}_{j,k}, \\ y &= \sum_{j=-\infty}^{\infty} \sum_{k=-\infty}^{\infty} B_{j,k} e^{i[2j\nu_1 + (2k+1)\nu_2]t}, \quad B_{-j,-k-1} = \bar{B}_{j,k}. \end{aligned} \tag{24}$$

This is the case for box orbits (Ratcliff, Chang, and Schwarzschild, 1984) while for loop orbits, for which the most prominent motion in both x and y is the circulation about the center, both series have the same form

$$x = \sum_{j=-\infty}^{\infty} \sum_{k=-\infty}^{\infty} A_{j,k} e^{i[(2j+1)\nu_1 + k(\nu_1+\nu_2)]t}, \quad A_{-j-1,-k} = \bar{A}_{j,k},$$
$$y = \sum_{j=-\infty}^{\infty} \sum_{k=-\infty}^{\infty} B_{j,k} e^{i[(2j+1)\nu_1 + k(\nu_1+\nu_2)]t}, \quad B_{-j-1,-k} = \bar{B}_{j,k}. \quad (25)$$

Orbits have another symmetry. If they are started on the x-axis at their maximum excursion in x with initial conditions $x = x_{\max}$, $\dot{x} = 0$, and $y = 0$, then the solutions for x and y are respectively even and odd in t. Hence x has a cosine series and y a sine series. An orbit which is started at some other time will reach $x = x_{\max}$ at time $t = t_0$ say, and so its x and y are even and odd in $(t - t_0)$. Consequently the Fourier coefficients of (24) have the forms

$$A_{j,k} = \pm |A_{j,k}| e^{-i[(2j+1)\nu_1 + 2k\nu_2]t_0}, \quad B_{j,k} = \pm |B_{j,k}| e^{i[\pi/2 - 2j\nu_1 t_0 - (2k+1)\nu_2 t_0]}, \quad (26)$$

for some unknown t_0, and similar formulas apply to loop orbits. The arguments of the complex Fourier coefficients allow us to deduce the values of both $\nu_1 t_0$ and $\nu_2 t_0$, though only modulo π.

4.2.1. *A box orbit*

Our estimates of the fundamental x and y frequencies for the box orbit which is at $x = 0.49$, $\dot{x} = 1.3156$, $y = 0$, $\dot{y} = 0.4788$, at $t = 0$ are found from an integration with $T = 100$ and $N = 4096$, as

$$\nu_1 = 2.16322769, \qquad \nu_2 = 3.01399443. \quad (27)$$

There are 53 conjugate pairs of amplitudes $A_{j,k}$ and 51 conjugate pairs of $B_{j,k}$ whose magnitudes exceed 10^{-5}. The ten largest are listed in Table II, and one member of each pair is displayed in Fig. 4. Only a few terms in k are needed, but many more in j because the decay in j resembles that in the one-dimensional orbit of Section 4.1. Summing the partial series (24) using the coefficients of magnitude greater than 10^{-5} reproduces the orbit with average errors of 3×10^{-5} at each tabular point.

We can use the Fourier coefficients to calculate the two actions and to verify the Hamiltonian constraints. Equations (4) and (5) require that

$$\sum_{j=-\infty}^{\infty} \sum_{k=-\infty}^{\infty} \{(2j+1)\,[(2j+1)\nu_1 + 2(k-m)\nu_2]\, A_{j,k} A_{-j-1,m-k}$$

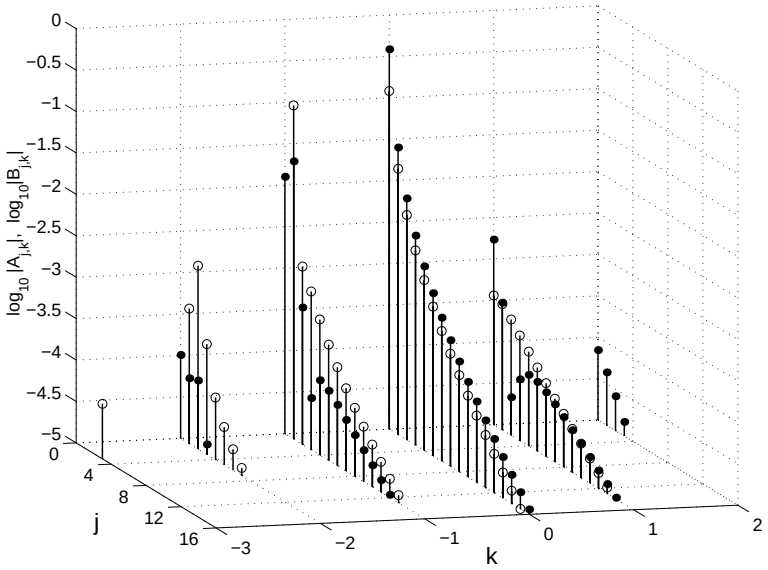

Figure 4. Magnitudes of Fourier coefficients for x, filled circles, and y, open circles, for the box orbit. There are open circles for all $0 \le j \le 13$, $k = 1$, but some are hidden by overlapping filled circles.

Table II. The ten largest Fourier coefficients of the box series (24) for the frequencies (27). The arguments are consistent with equation (26) and the values $\nu_1 t_0 = 1.03468 \pmod{\pi}$ and $\nu_2 t_0 = 1.00447 \pmod{\pi}$.

j	k	$\lvert A_{j,k}\rvert$	$\arg A_{j,k}$	j	k	$\lvert B_{j,k}\rvert$	$\arg B_{j,k}$
0	0	0.38565023	5.24850	0	0	0.12072946	3.70791
1	0	0.02912085	0.03754	1	-1	0.10684730	0.50590
1	-1	0.02252003	5.18808	1	0	0.01611545	4.78014
0	-1	0.01264537	0.97426	2	0	0.00517818	5.85237
2	0	0.00821225	1.10977	3	0	0.00224771	0.64141
3	0	0.00338263	2.18199	2	-2	0.00163069	0.44548
0	1	0.00171443	0.09796	2	-1	0.00140476	4.71972
4	0	0.00167051	3.25422	4	0	0.00113731	1.71363
5	0	0.00091742	4.32644	3	-1	0.00081479	5.79195
6	0	0.00054005	5.39867	5	0	0.00063138	2.78586

$$
\begin{aligned}
&+2j\left[2j\nu_1+(2k-2m+1)\nu_2\right]B_{j,k}B_{-j,m-k-1}\}=\delta_{mo}I_1,\\
\sum_{j=-\infty}^{\infty}\sum_{k=-\infty}^{\infty}&\{2k\left[(2j-2m+1)\nu_1+2k\nu_2\right]A_{j,k}A_{m-j-1,-k}\\
&+(2k+1)\left[2(j-m)\nu_1+(2k+1)\nu_2\right]B_{j,k}B_{m-j,-1-k}\}=\delta_{mo}I_2.
\end{aligned}
\tag{28}
$$

The constraints are satisfied to an accuracy which is consistent with the truncations of the Fourier series, and the actions are $I_1 = 0.76050$, $I_2 = 0.06422$.

4.2.2. *A loop orbit*

The two most prominent frequencies of the loop orbit which begin from $x = 0.49$, $\dot{x} = 0.4788$, $y = 0$, $\dot{y} = 1.3156$, found from an integration with $T = 50$ and $N = 2048$, are

$$\nu_1 = 2.948610113, \qquad \nu_2 = 1.357500105. \tag{29}$$

These two fundamental frequencies are related to the frequencies Ω and $\kappa - \Omega$ of epicyclic motion ((Binney and Tremaine, 1987), Chapter 3). They are more easily determined accurately for this orbit which keeps away from the core, and for which the Fourier series converge faster. There are 42 conjugate pairs of amplitudes $A_{j,k}$ and 43 pairs of amplitudes $B_{j,k}$ whose magnitudes exceed 10^{-6}. The ten largest are listed in Table III, and one member of each pair is displayed in Fig. 5. Amplitudes decay more rapidly with j than with k. Summing the partial series (25) using the coefficients of magnitude greater than 10^{-6} reproduces the orbit with average errors of 3×10^{-6} at each tabular point.

When equations (4) and (5) are applied to the series (25), we get the conditions

$$
\begin{aligned}
&\sum_{j=-\infty}^{\infty}\sum_{k=-\infty}^{\infty}(2j+k+1)\left[(2j+k+1)\nu_1+k\nu_2\right](A_{j,k}A_{-j-1-m,2m-k}\\
&\quad+B_{j,k}B_{-j-1-m,2m-k})=\delta_{mo}I_1,\\
&\sum_{j=-\infty}^{\infty}\sum_{k=-\infty}^{\infty}k\left[(2j+k+1)\nu_1+k\nu_2\right](A_{j,k}A_{m-j-1,-k}\\
&\quad+B_{j,k}B_{m-j-1,-k})=\delta_{mo}I_2.
\end{aligned}
\tag{30}
$$

The constraints are well satisfied in this case because of the more convergent Fourier series, and the actions are $I_1 = 0.62879$, $I_2 = 0.04366$.

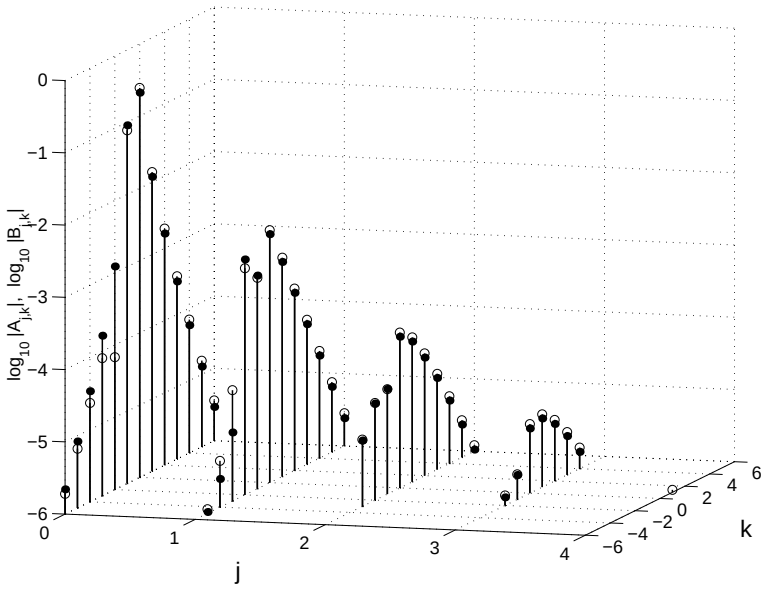

Figure 5. Magnitudes of Fourier coefficients for x, filled circles, and y, open circles, for the loop orbit. Three open circles at $j = 2$ and two at $j = 3$ are hidden by overlapping filled circles.

Table III. The ten largest Fourier coefficients of the loop series (25) for the frequencies (29). The arguments are consistent with $\nu_1 t_0 = .33891 \pmod{\pi}$ and $\nu_2 t_0 = 1.08622 \pmod{\pi}$ and equation (25).

j	k	$\lvert A_{j,k}\rvert$	$\arg A_{j,k}$	j	k	$\lvert B_{j,k}\rvert$	$\arg B_{j,k}$
0	0	0.21093349	5.94428	0	0	0.24538048	4.37348
0	-1	0.09038719	1.08622	0	-1	0.07740396	5.79861
0	1	0.01189380	1.37755	0	1	0.01382317	6.08994
1	0	0.00273923	5.26646	1	0	0.00313257	3.69566
1	-2	-0.00181571	1.83354	0	2	0.00187210	1.52321
0	2	-0.00160147	3.09401	1	-2	0.00137322	0.26275
0	-2	0.00122769	5.65295	1	1	0.00106544	5.41212
1	1	0.00093184	0.69973	1	-1	0.00082623	5.12079
1	-1	0.00089276	0.40841	0	3	0.00033780	3.23967
0	3	0.00028643	4.81047	1	2	0.00032815	0.84539

5. Discussion

5.1. Comparisons with NAFF

The discrete transform procedure described in this paper resembles NAFF in its basic approach in that it assumes quasi-periodic motion and seeks to calculate an adequate description of that motion. It is more streamlined than existing procedures. A single discrete Fourier transform is taken once and there is no need to either calculate Fourier integrals, maximize them, or for orthogonal projection. Test calculations show that the procedure attains high accuracy in estimating frequencies and amplitudes, and frequency components do not need to be subtracted twice (Laskar, 1993).

Laskar (1999) proves a theorem which shows that his procedure of locating the maximum of $|\phi(\sigma)|$, where the function $\phi(\sigma)$ is defined as

$$\phi(\sigma) = \frac{1}{2T} \int_{-T}^{T} f(t) \chi_p \left(\frac{t}{T} \right) e^{-i\sigma t} dt, \tag{31}$$

locates the most prominent frequency to within $O(1/T^{2p+2})$. This proof assumes that the integral for $\phi(\sigma)$, which has in practice to be evaluated numerically because values of f are known only at tabular points, is known exactly. It is evident that all but one of the orders of T^{-1} in the accuracy come from the windowing, and only the final $(2p+2)$'th from the maximization. Laskar's standard choice is $p = 1$; he reports trying other p values, but not noting much improvement. We do find significant improvements with the use of larger p, and have much success with p in the range of 3 to 5. Our iterative procedure does not lock us into any *a priori* choice of p, and we can check for convergence and consistency.

We differ from Laskar in that we fit the Fourier series for $\mathbf{x}$, whereas he fits the complex combination $\mathbf{x} + i\mathbf{v}$, which has Fourier coefficients $(1 - \mathbf{k} \cdot \nu)\mathbf{X_k}$. The series for $\mathbf{x}$ has the somewhat more rapidly decaying coefficients which should make it easier to fit. The velocity vector $\mathbf{v}$ cannot contain any significant information that is not in $\mathbf{x}$ because both are computed simultaneously from accurate numerical integration of an orbit – we use the DOP 853 integrator of Hairer and Wanner (Hairer, Norsett, and Wanner, 1991). Hence we see no reason why fitting $\mathbf{x} + i\mathbf{v}$ should be any improvement over fitting $\mathbf{x}$.

5.2. Summary and Conclusions

We have shown how the spectral analysis of orbits can be carried out wholly, efficiently and accurately using the DFT. We have given examples, and have investigated the rates of convergence of their Fourier series. This may be slow if the motion in the orbit is far from sinusoidal in time, and an impractically large number of terms may then be needed for an accurate Fourier representation.

There are two choices which have to be made at the outset, the duration $2T$ of the integration and the number $2N$ of outputs. The DOP 853 routine makes it easy to obtain frequent output, and hence to make N sufficiently large to avoid complications from aliasing. The choice of T is significant because the inverse of the DFT (6) is

$$f(t) = \sum_{k=1-N}^{N} F_k e^{\pi i k t/T}. \tag{32}$$

We need T to be sufficiently large that $|\Delta\nu|T/\pi$ is large for the difference $|\Delta\nu|$ between any pair of frequencies which are significant in the spectrum, so that they are represented by well-separated k values in expansion (32). We also need $\pi N/T$, the highest frequency in expansion (32) to be large enough that all the frequencies which are present in the true solution are represented in its discrete approximation.

Copin, Zhao, and de Zeeuw (2000) have shown that orbital density is proportional to the reciprocal of the Jacobian of the transformation between position and angles for that orbit. That Jacobian is known from the Fourier series (1), and allows orbital densities, which are needed to construct stellar dynamic models, to be calculated significantly more accurately than is possible with the binning methods (Schwarzschild, 1979) that have been used for so long. The DFT method, which gives a fast and accurate way of determining the Fourier series (1), therefore has great potential for applications to galactic modeling.

Appendix

We show here that the equation

$$G_{k-1}^{(p)}(\theta) = CG_k^{(p)}(\theta), \tag{33}$$

for determining θ, and thence the frequency ν, is a polynomial equation of degree $2p$ in $\tan(\theta/2N)$. It follows from equation (11) that

$$G_k(\theta) = \frac{\sin\theta}{2N\tau}, \quad G_{k+\ell}(\theta) = \frac{(-1)^\ell \sin\theta}{2N} \frac{1+\tau\tau_\ell}{\tau-\tau_\ell}, \tag{34}$$

where

$$\tau = \tan\frac{\theta}{2N}, \quad \tau_\ell = \tan\frac{\ell\pi}{2N}. \tag{35}$$

The iterated coefficient $G_k^{(p)}$ can be related directly to the basic G-coefficients by repeated application of relation (10), or more directly by expanding equation (7) binomially using equation (8), to get

$$\begin{aligned} G_k^{(p)} &= \frac{(p!)^2}{(2p)!}\sum_{\ell=-p}^{p}\binom{2p}{\ell+p}G_{k+\ell} \\ &= \frac{\sin\theta}{2N\tau}\left[1+\sum_{\ell=1}^{p}\frac{(-1)^\ell(p!)^2}{(p-\ell)!(p+\ell)!}\frac{2(1+\tau_\ell^2)\tau^2}{\tau^2-\tau_\ell^2}\right] \end{aligned} \tag{36}$$

In passing from the first line to the second, we have combined $G_{k\pm\ell}$ terms in pairs. The term in the square brackets is the ratio of two polynomials of degree p in τ^2. Its numerator has $(1+\tau^2)$ as a factor because it vanishes when $\tau^2 = -1$. This is seen by setting $\tau^2 = -1$, and recognizing the sum as the binomial expansion of $(p!)^2(1-1)^{2p}/(2p)! = 0$.

The other iterated coefficient of

$$G_{k-1}^{(p)} = \frac{(p!)^2}{(2p)!}\sum_{\ell=-p}^{p}\binom{2p}{\ell+p}G_{k-1+\ell}, \tag{37}$$

is less symmetric in τ, but it is likewise rational in τ with a numerator polynomial of degree $2p$ divided by a denominator polynomial of degree $(2p+1)$. Its denominator differs from that of $G_k^{(p)}$ only in having a factor $(\tau - \tau_{-p-1})$ and lacking one in $(\tau - \tau_p)$. Furthermore the numerator of $G_{k-1}^{(p)}$ also has $(1+\tau^2)$ as a factor. This follows from the alternative and symmetric expression for it we get from equation (36) when we replace τ by $\tilde{\tau} = \tan[(\theta+\pi)/2N] = (\tau+\tau_1)/(1-\tau\tau_1)$, because $(1+\tilde{\tau}^2) = (1+\tau^2)(1+\tau_1^2)/(1-\tau\tau_1)^2$. Consequently when we multiply equation (33) by all denominator terms and cancel all common factors, a polynomial equation of degree $2p$ in τ remains.

Acknowledgements

It is a pleasure to thank Alex Fridman for organizing a stimulating workshop, and him and the Director and staff of the Sternberg Astronomical Institute for their hospitality. This work has been supported in part by the National Science Foundation through grant DMS-9704615.

References

Binney, J. and D. Spergel. Spectral stellar dynamics, *Astrophys. J.*, 252:308-321, 1982.

Binney, J. and D. Spergel. Spectral stellar dynamics - II. The action integrals, *Monthly Notices Royal Astron. Soc.*, 206:159-177, 1984.

Binney, J. and S. Tremaine. *Galactic Dynamics.* Princeton Univ. Press, Princeton, NJ, USA, 1987.

Briggs, W. L. and V. E. Henson. *The DFT: an owner's manual of the discrete Fourier transform.* Society for Industrial and Applied Mathematics, Philadelphia, PA, USA, 1995.

Carpintero, D. D. and L. A. Aguilar. Orbit classification in arbitrary 2D and 3D potentials, *Monthly Notices Royal Astron. Soc.*, 298:1-21, 1998.

Copin, Y., H. S. Zhao, and P. T. de Zeeuw. Probing a regular orbit with spectral dynamics, *Monthly Notices Royal Astron. Soc.*, 318:781-797, 2000.

Davis, P. J. *Interpolation and Approximation.* Dover, New York, NY, USA, 1975.

Hairer, E., S. P. Norsett, and G. Wanner. *Solving Ordinary Differential Equations I.* Springer Verlag, New York, NY, USA, 1991.

Lanczos, C. *Applied Analysis.* Prentice Hall, Englewood Cliffs, NJ, USA, 1956.

Laskar, J. The chaotic motion of the solar system: a numerical estimate of the size of the chaotic zones, *Icarus*, 88: 266-291, 1990.

Laskar, J. Frequency analysis for multi-dimensional systems. Global dynamics and diffusion, *Physica D*, 67: 257-281, 1993.

Laskar, J. Introduction to frequency map analysis In C. Siwo, editor, *Hamiltonian Systems with Three or more Degrees of Freedom.* Kluwer, Dordrecht, Netherlands, 1999.

Merritt, D. and M. Valluri. Resonant orbits in triaxial galaxies, *Astron. J.*, 118:1177-1189, 1999.

Papaphilippou, Y. and J. Laskar. Frequency map analysis and global dynamics in a galactic potential with two degrees of freedom, *Astron. Astrophys.*, 307:427-449, 1996.

Papaphilippou, Y. and J. Laskar. Global dynamics of triaxial galactic models through frequency map analysis, *Astron. Astrophys.*, 329:451-481, 1998.

Ratcliff, S. J., K. M. Chang, and M. Schwarzschild. Stellar orbits in angle variables, *Astrophys. J.*, 279:610-620, 1984.

Schwarzschild, M. A numerical model for a triaxial stellar system in dynamical equilibrium, *Astrophys. J.*, 232:236-247, 1979.

Valluri, M. and D. Merritt. Regular and chaotic dynamics of triaxial stellar systems, *Astrophys. J.*, 506:686-711, 1998.

Wachlin, F. C. and S. Ferraz-Mello. Frequency map analysis of the orbital structure in elliptical galaxies, *Monthly Notices Royal Astron. Soc.*, 298:22-32, 1998.